

## CP violating asymmetry in $H^\pm \rightarrow W^\pm h_1$ decays

W. Hollik and D.T. Nhung

*Max-Planck-Institut für Physik (Werner-Heisenberg-Institut),  
D-80805 München, Germany*

### Abstract

The CP violating asymmetry from the decay rates  $H^\pm \rightarrow W^\pm h_1$  of charged Higgs bosons into the lightest neutral Higgs boson and a  $W^\pm$  boson is calculated and discussed in the complex MSSM. The contributions from all complex phases are considered, especially from the top-squark trilinear coupling, which induces a large contribution to the CP asymmetry.

# 1 Introduction

In the Minimal Supersymmetric Standard model with complex parameters (complex MSSM), new sources of CP violation are associated with the phases of the soft-breaking parameters and of the Higgsino-mass parameter  $\mu$ . Through loop contributions, CP violation also enters the Higgs sector, which is CP conserving at lowest order (see for example [1] for a detailed study and references). As a consequence, the  $h, H$  and  $A$  neutral Higgs bosons in general mix and form the neutral mass eigenstates  $h_{1,2,3}$  with both CP even and odd properties, giving rise to CP-violation in suitable observables, like decay rates of charged particles. An interesting decay mode is given by the charged Higgs boson decays  $H^- \rightarrow W^- h_1$  and  $H^+ \rightarrow W^+ h_1$ , where the asymmetry between the decay rates is a CP-violating observable. A first calculation was done in [2], studying the CP asymmetry as derived from the phases of the trilinear  $\tilde{\tau}$  coupling,  $A_\tau$ , and of  $M_1$ , yielding asymmetries of the order  $10^{-2}$ ; contributions from the quark/squark sector were not included.

In this paper we extend the calculation of [2] including contributions from all physical phases in the general complex MSSM with minimal flavor violation, in particular from  $A_t$  and  $A_b$ , which enter through Feynman diagrams with stops and sbottoms involving large Yukawa couplings, further enhanced by the color factor. We show the results from the complete set of one-loop diagrams, including besides the Higgs self energies all the loop contributions to the  $H^\pm \rightarrow W^\pm h_1$  vertex, which at lowest order is in general suppressed by a factor  $\cos(\beta - \alpha)$ .

The paper is organized as follows. We first outline in section 2, the structure of the complex MSSM neutral Higgs bosons. In section 3, we indicate the calculation of the CP decay rate asymmetry. A discussion of the results follows in section 4, and conclusions in section 5.

## 2 The Higgs sector of the complex MSSM

In the MSSM, CP violation arises from the Yukawa sector and the soft SUSY-breaking sector through complex couplings. Physical phases are the phase of the trilinear couplings  $A_f$ , of the higgsino parameter  $\mu$ , of the gaugino mass parameters  $M_i$  ( $i = 1, 2, 3$ ),

$$A_f = |A_f|e^{i\phi_f}, \quad \mu = |\mu|e^{i\phi_\mu}, \quad M_i = |M_i|e^{i\phi_i}, \quad (1)$$

and the CKM phase as in the Standard Model. The phase of the CKM matrix has a very small impact on the CP asymmetry considered here and is neglected in the following. At tree level, the complex SUSY phases enter the mass matrices of squarks, sleptons, charginos and neutralinos. In the Higgs sector, CP violation effects enter only at the loop level.

### Tree level:

Using the conventions of [3], we write the two Higgs doublets in the form

$$\mathcal{H}_1 = \begin{pmatrix} v_1 + \frac{1}{\sqrt{2}}(\phi_1 - i\chi_1) \\ -\phi_1^- \end{pmatrix}, \quad \mathcal{H}_2 = \begin{pmatrix} \phi_2^+ \\ v_2 + \frac{1}{\sqrt{2}}(\phi_2 + i\chi_2) \end{pmatrix}, \quad (2)$$

with the vacuum expectation values  $v_1, v_2$ , yielding the ratio  $\tan\beta = v_2/v_1$ . The mass eigenstates are related to the field components in (2) by unitary matrices, for the neutral

Higgs case given by

$$\begin{pmatrix} h \\ H \\ A \\ G \end{pmatrix} = \begin{pmatrix} -\sin \alpha & \cos \alpha & 0 & 0 \\ \cos \alpha & \sin \alpha & 0 & 0 \\ 0 & 0 & -\sin \beta_n & \cos \beta_n \\ 0 & 0 & \cos \beta_n & \sin \beta_n \end{pmatrix} \begin{pmatrix} \phi_1 \\ \phi_2 \\ \chi_1 \\ \chi_2 \end{pmatrix}, \quad (3)$$

and for the charged Higgs fields by

$$\begin{pmatrix} H^\pm \\ G^\pm \end{pmatrix} = \begin{pmatrix} -\sin \beta_c & \cos \beta_c \\ \cos \beta_c & -\sin \beta_c \end{pmatrix} \begin{pmatrix} \phi_1^\pm \\ \phi_2^\pm \end{pmatrix}, \quad (4)$$

with  $\beta_n = \beta_c = \beta$ . At the tree level, the Higgs potential conserves CP, hence the CP-even states  $h, H$  do not mix with the CP-odd states  $A$ .

### Higher order:

Through the nonvanishing CP phases in the loop contributions mixing between  $h, H$  and  $A$  occurs. Moreover, there is mixing of the neutral Higgs bosons with  $G$  and  $Z$ , but they yield only sub-leading two-loop contributions to the Higgs boson masses, see e.g. [3]. The lowest-order mass eigenvalues  $m_h, m_H$  and  $m_A$  are different from the pole masses. The loop-corrected masses (pole masses) of the neutral Higgs are obtained via the poles of the propagator matrix,

$$\Delta_{hHA} = -[\hat{\Gamma}_{hHA}(p^2)]^{-1}, \quad (5)$$

with

$$\begin{aligned} \hat{\Gamma}_{hHA}(p^2) &= i[p^2 - M(p^2)], \\ M(p^2) &= \begin{pmatrix} m_h^2 - \hat{\Sigma}_{hh}(p^2) & -\hat{\Sigma}_{hH}(p^2) & -\hat{\Sigma}_{hA}(p^2) \\ -\hat{\Sigma}_{hH}(p^2) & m_H^2 - \hat{\Sigma}_{HH}(p^2) & -\hat{\Sigma}_{HA}(p^2) \\ -\hat{\Sigma}_{hA}(p^2) & -\hat{\Sigma}_{HA}(p^2) & m_A^2 - \hat{\Sigma}_{AA}(p^2) \end{pmatrix}, \end{aligned} \quad (6)$$

where  $\hat{\Sigma}_{ij}$  ( $i, j = h, H, A$ ) are the renormalized self-energies in the scheme of [3], which treats the renormalization of the Higgs fields and of  $\tan \beta$  according to the  $\overline{\text{DR}}$  prescription. In general, the three poles are complex and written as

$$\mathcal{M}_{h_a}^2 = M_{h_a}^2 - iM_{h_a}\Gamma_{h_a}, \quad a = 1, 2, 3, \quad (7)$$

where  $M_{h_a}$  are the loop-corrected masses with the convention

$$M_{h_1} < M_{h_2} < M_{h_3}, \quad (8)$$

and  $\Gamma_{h_a}$  are the corresponding total decay widths. The mass of the charged Higgs-boson is chosen as an input parameter and is renormalized on-shell. Again, there is also mixing between  $H^\pm$  and  $G^\pm, W^\pm$  at one-loop order, which has to be taken into account in processes with external charged Higgs bosons.

### 3 Decay widths and CP asymmetry

The CP violating asymmetry in the charged-Higgs decay into a  $W$ -boson and the lightest neutral Higgs,  $h_1$ , is defined in the following way

$$\delta_{\text{CP}} = \frac{\Gamma(H^- \rightarrow W^- h_1) - \Gamma(H^+ \rightarrow W^+ h_1)}{\Gamma(H^- \rightarrow W^- h_1) + \Gamma(H^+ \rightarrow W^+ h_1)} \quad (9)$$

in terms of the individual partial decay widths  $\Gamma(H^\pm \rightarrow W^\pm h_1)$ . Writing the decay amplitudes as follows,

$$\mathcal{A}(H^\pm \rightarrow W^\pm h_1) = (\epsilon_\lambda \cdot p_{H^\pm}) \mathcal{M}(H^\pm \rightarrow W^\pm h_1) \quad (10)$$

with the  $W$  polarization vectors  $\epsilon_\lambda$  and the  $H^\pm$  momentum  $p_{H^\pm}$ , the decay widths integrated over the 2-particle phase space and summed over the  $W$  helicities  $\lambda$  are obtained in the form

$$\Gamma(H^\pm \rightarrow W^\pm h_1) = R_2 \cdot |M_{H^\pm \rightarrow W^\pm h_1}|^2, \quad (11)$$

with

$$R_2 = \frac{\lambda^{3/2}(M_{H^\pm}^2, M_W^2, M_{h_1}^2)}{64\pi M_{H^\pm}^3 M_W^2}, \quad \lambda(x, y, z) = x^2 + y^2 + z^2 - 2xy - 2xz - 2yz. \quad (12)$$

The decay amplitude at higher order can be written in the following way,

$$\begin{aligned} \mathcal{M}_{H^\pm \rightarrow W^\pm h_1} &= \sqrt{Z_{H-H^+}} [\mathbf{Z}_{11} (M_{H^\pm \rightarrow W^\pm h}^{\text{tree}} + \delta M_{H^\pm \rightarrow W^\pm h}) \\ &\quad + \mathbf{Z}_{12} M_{H^\pm \rightarrow W^\pm H}^{\text{tree}} + \mathbf{Z}_{13} M_{H^\pm \rightarrow W^\pm A}^{\text{tree}}], \end{aligned} \quad (13)$$

with the tree-level expressions  $M^{\text{tree}}$  given by (with  $s_W = \sin \theta_W$ )

$$M_{H^\pm \rightarrow W^\pm h}^{\text{tree}} = \frac{e \cos(\beta - \alpha)}{s_W}, \quad M_{H^\pm \rightarrow W^\pm H}^{\text{tree}} = -\frac{e \sin(\beta - \alpha)}{s_W}, \quad M_{H^\pm \rightarrow W^\pm A}^{\text{tree}} = \pm i \frac{e}{s_W}, \quad (14)$$

the charged-Higgs wave function renormalization  $\sqrt{Z_{H-H^+}}$ , the neutral-Higgs wave function renormalization factors  $\mathbf{Z}_{kl}$ , and

$$\delta M_h \equiv \delta M_{H^\pm \rightarrow W^\pm h} = \delta M_{H^\pm \rightarrow W^\pm h}^{1\text{PI}} + \delta M_{H^\pm \rightarrow W^\pm h}^{G, W \text{mix}} \quad (15)$$

which summarize the residual 1PI-irreducible contributions to the 3-point vertex function and the mixing of  $H^\pm$  with  $G^\pm$  and  $W^\pm$ . The Feynman diagrams contributing to this term at the one-loop level are shown in figure 1. There is no explicit wave function renormalization for the  $W$  boson, since the  $W$  propagator has been renormalized on-shell yielding residue = 1.

The Higgs fields  $H^\pm$ ,  $h_1$  and  $\tan \beta$  are renormalized in  $\overline{\text{DR}}$  scheme. The correct on-shell properties of the S-matrix element involving external neutral Higgs bosons are ensured by the inclusion of the wave function renormalization factors summarized in the matrix  $\mathbf{Z}$ , as given in [3]:

$$\mathbf{Z} = \begin{pmatrix} \sqrt{Z_h} & \sqrt{Z_h} Z_{hH} & \sqrt{Z_h} Z_{hA} \\ \sqrt{Z_H} Z_{Hh} & \sqrt{Z_H} & \sqrt{Z_H} Z_{HA} \\ \sqrt{Z_A} Z_{Ah} & \sqrt{Z_A} Z_{AH} & \sqrt{Z_A} \end{pmatrix}, \quad (16)$$

where  $(i, j = h, H, A)$

$$\begin{aligned} Z_i &= \frac{1}{\left(\frac{i}{\Delta_{ii}(p^2)}\right)'(M_i^2)}, \\ Z_{ij} &= \frac{\Delta_{ij}(p^2)}{\Delta_{ii}(p^2)} \Big|_{p^2=M_i^2}, \end{aligned} \quad (17)$$

involving the elements  $\Delta_{ij}$  of the the propagator matrix  $\Delta_{hHA}$  in (5).

For the charged Higgs boson, the wave function renormalization is derived from

$$Z_{H^-H^+} = \left[1 + \text{Re} \frac{\partial}{\partial p^2} \hat{\Sigma}_{H^-H^+}\right]^{-1}_{p^2=M_{H^\pm}^2}, \quad (18)$$

with the  $\overline{\text{DR}}$ -renormalized self-energy  $\hat{\Sigma}_{H^-H^+}$ . At one-loop order we get

$$\begin{aligned} Z_{H^-H^+} &\simeq 1 - \text{Re} \frac{\partial}{\partial p^2} \hat{\Sigma}_{H^-H^+} \Big|_{p^2=M_{H^\pm}^2} \equiv 1 - \delta Z_{H^-H^+}, \\ \sqrt{Z_{H^-H^+}} &\simeq 1 - \frac{1}{2} \delta Z_{H^-H^+}. \end{aligned} \quad (19)$$

The factor  $Z_{H^-H^+}$  is IR-divergent. We regularise the IR-divergence in the one-loop expanded version with the help of a small photon mass, to be canceled by including real photon bremsstrahlung.

Substituting the amplitude (13) into the expression (11), one obtains the decay width, denoted as  $\Gamma_{\mathbf{Z}}^{(0+1+2)}$  later in the paper. Keeping the  $\mathbf{Z}$  factors in the squared amplitude is justified since they contain also the leading higher-order terms which correspond to the effective-potential approximation. In the squared one-loop amplitude, we also keep the term involving  $\delta M_h^2$ . This term can play an important role at large value of  $M_{H^-}$ , *i.e.*  $M_{H^-} \geq M_{\tilde{t}_1} + M_{\tilde{b}_1}$ , where the decay channel into  $\tilde{t}_1$  and  $\tilde{b}_1$  is open, while it is negligible at lower  $M_{H^-}$ . The inclusion of this term while neglecting other two-loop contributions is consistent in perturbation theory, since the tree-level vertex function  $M_h^{\text{tree}} \sim \cos(\beta - \alpha) \sim M_Z^2/M_{H^-}^2$  goes to near zero at large  $M_{H^-}$ . The IR divergence at the one-loop level is canceled by adding the real photon radiation contribution. An IR-divergence in the squared one-loop term is avoided by taking only the (s)top/(s)bottom diagrams which are IR finite and give the dominant contributions, as checked in [4].

In practice, there are two ways to compute the CP asymmetry: (i) to compute both decay widths of  $H^- \rightarrow W^- h_1$  and of the CP-conjugate process  $H^+ \rightarrow W^+ h_1$  and then using the definition (9); (ii) to compute separately the CP-violating and the CP-invariant contributions to the decay  $M_{H^- \rightarrow W^- h_1}$  and then taking their ratio. The CP-violating term comes from the imaginary part of the complex couplings (together with the imaginary part of the loop integrals), while the CP-invariant term is from the real part. Therefore the CP-violating term change sign, but the CP-invariant term does not when going from  $H^- \rightarrow W^- h_1$  to  $H^+ \rightarrow W^+ h_1$ . Hence, one can identify the Feynman diagrams shown in figure 2 as those contributing to the CP-violating part.

We have performed our calculation in the two ways, with perfect agreement. The full result for  $\delta_{CP}$  is obtained when both the numerator and denominator of the asymmetry (9) are

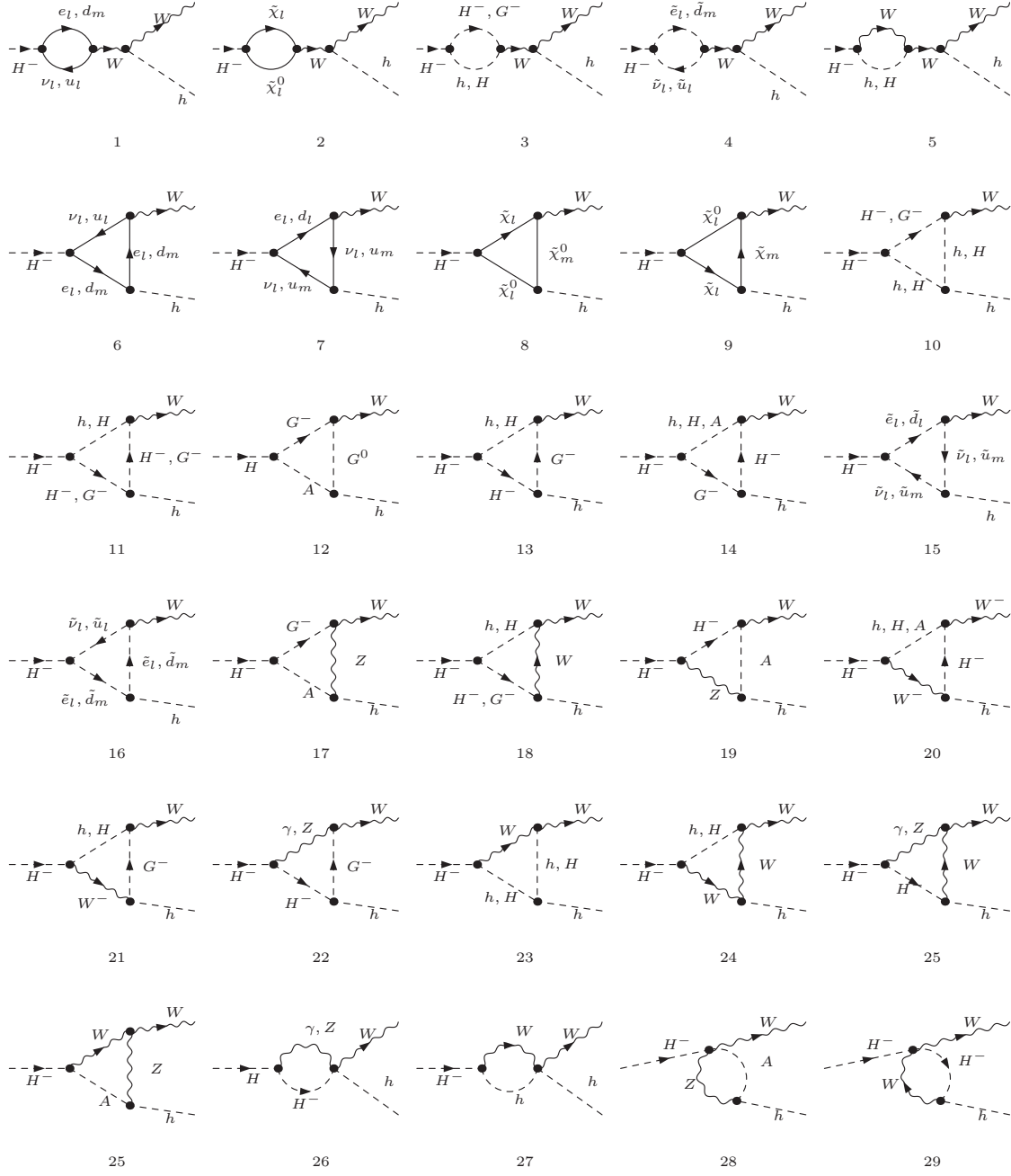


Figure 1: One-loop Feynman diagrams contribute to  $\delta M_h$

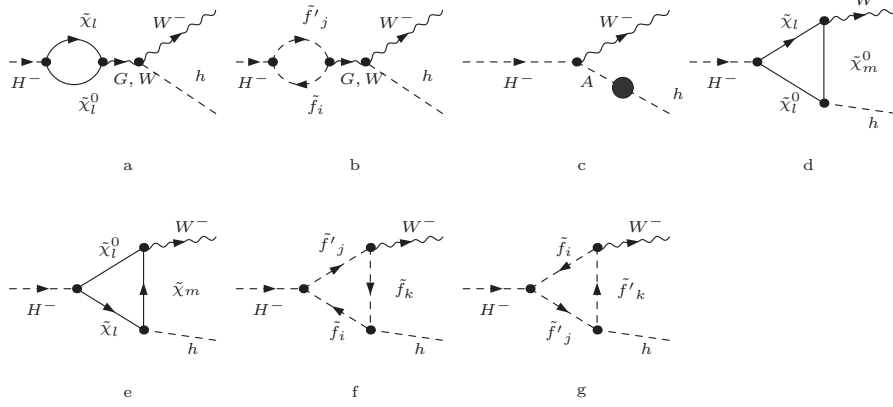


Figure 2: Feynman diagrams contain weak phases which contribute to the CP rate asymmetry

computed with the inclusion of higher order terms. This is different with the approximation used in Ref. [2] where the numerator is computed at strict one-loop order and the denominator is tree-level like, and is necessary since in specific case the process is loop dominated, as we will illustrate in the numerical analysis.

For comparison with other approximations, we introduce the following notations for decay width:

- The improved Born approximation for the decay width  $\Gamma_{\mathbf{Z}}^{(0)}$  with the  $\mathbf{Z}$  factors taken into account:

$$\Gamma_{\mathbf{Z}}^{(0)} = R_2 \cdot \left| \sum_i \mathbf{Z}_{1i} M_i^{\text{tree}} \right|^2, \quad i = h, H, A. \quad (20)$$

- The one-loop improved decay width  $\Gamma_{\mathbf{Z}}^{(0+1)}$  that does not include  $\delta M_h^2$ :

$$\Gamma_{\mathbf{Z}}^{(0+1)} = R_2 \cdot \left[ \left| \sum_i \mathbf{Z}_{1i} M_i^{\text{tree}} \right|^2 + 2 \sum_i |\mathbf{Z}_{11}^* \mathbf{Z}_{1i} M_i^{\text{tree}} (\delta M_h - \frac{1}{2} M_h^{\text{tree}} \delta Z_{H-H^+})^*| \right]. \quad (21)$$

## 4 Numerical analysis

### 4.1 Calculational frame work

We have used **FeynArts** 3.4 [5] to generate the Feynman diagrams. In order to include the relevant counterterms, we have adapted the MSSM model file in FeynArts. The amplitudes are further evaluated by **FormCalc** 6.0 and the one-loop integrals are computed with the library **LoopTools** 2.4 [6]. All the dependent couplings and masses of internal lines are computed with tree-level relations. The mass of the external neutral Higgs is calculated by using **FeynHiggs** 2.6.5 [7]. In **FeynHiggs** 2.6.5, one has possibility to include various

important two-loop contributions to the renormalized self-energies. We have included the full-phase-dependent  $\alpha_s\alpha_t$  corrections and the  $(\alpha_s\alpha_b, \alpha_t\alpha_t, \alpha_t\alpha_b)$  corrections which are interpolated in the complex phases. Therefore, the most up-to-date higher-order renormalization factors  $\mathbf{Z}_{ij}$  are used in our calculation.

We should mention the problem of normal threshold singularities when  $M_{H^\pm}$  approaches the production threshold of two scalar particles, for instance up and down squarks. Following [8] and references therein, this problem can be overcome by using complex masses for the relevant unstable particles. In our case, the kinematical threshold of top and bottom squarks is concerned. This singularity appears in the renormalization factor of the charged Higgs boson,  $\delta Z_{H-H^+}$ , in particular in the derivative of two-point functions, which we treat according to the substitutions

$$\frac{d}{dp^2}B(p^2, M_{\tilde{t}_i}^2, M_{\tilde{b}_j}^2)\big|_{p^2=M_{H^\pm}^2} \quad \text{with} \quad \begin{cases} M_{H^\pm}^2 \rightarrow M_{H^\pm}^2 - iM_{H^\pm}\Gamma_{H^\pm}, \\ M_{\tilde{t}_i}^2 \rightarrow M_{\tilde{t}_i}^2 - iM_{\tilde{t}_i}\Gamma_{\tilde{t}_i}, \\ M_{\tilde{b}_j}^2 \rightarrow M_{\tilde{b}_j}^2 - iM_{\tilde{b}_j}\Gamma_{\tilde{b}_j}, \end{cases} \quad i, j = 1, 2. \quad (22)$$

The required decay widths have been computed in lowest order including all significant two-body decays.

Various cross checks of our calculation have been performed. Besides numerical and analytical checks of UV- and IR-finiteness, our results were checked versus those obtained by a independent calculation [4] for the real MSSM, and very good agreements has been found.

## 4.2 Input parameters

Our calculation is completely general, including all complex phases. However, there exist strong constraints on the CP violating parameter space. We chose  $\mu$  to be zero as default value in order to be consistent with the experimental data of the electric dipole moments. The phases of trilinear couplings of the first and second generations have marginal effects on the CP rate asymmetry because the masses of the corresponding fermions are small. In the following, those phases are also taken to be zero. The phase of  $M_3$ , which enters from two loop order, is set to be zero. The Standard Model input parameters are taken from [9]. The top mass  $m_t = 173.1$  GeV is taken from the most recent measurements [10]. The contributions of the CKM-phase to the CP rate asymmetry are negligible, thus the CKM matrix is set to be unit. For the soft SUSY breaking parameters and  $\mu$ , we use the following set as default values (unless specified otherwise),

$$\begin{aligned} \mu &= 200 \text{ GeV}, M_2 = 200 \text{ GeV}, M_3 = 0.8 M_{\text{SUSY}}, |A_\tau| = |A_t| = |A_b|, \\ M_{\tilde{Q}} &= M_{\tilde{D}} = M_{\tilde{U}} = M_{\text{SUSY}} = 500 \text{ GeV}, M_{\tilde{L}} = 200 \text{ GeV}, M_{\tilde{E}} = 150 \text{ GeV}. \end{aligned} \quad (23)$$

The values of  $\mu$  and  $M_3$  are chosen as in the  $m_h^{\text{max}}$  scenario to maximize the lightest neutral Higgs mass [11].  $M_1$  and  $M_2$  are chosen as connected via the GUT relation  $|M_1| = 5/3 \tan^2 \theta_W |M_2|$ . Because of this relation, we can set  $\phi_2 = 0$  while  $\phi_1$  is kept as a free parameter. The relevant Higgs and SUSY particle masses are shown in Table 1 (for  $M_{H^\pm} = 300$  GeV and  $|A_t| = 800$  GeV). Also when varying the parameters, we have always obeyed the



Table 1: Masses of Higgs bosons and SUSY particles (in GeV) for the parameter set (23) and  $\phi_1 = \phi_\tau = \phi_t = \phi_b = \pi/2$ ,  $|A_t| = 800$  GeV.

$\tan \beta$	$M_{H^\pm}$	$M_{h_1}$	$M_{\tilde{\nu}}$	$M_{\tilde{\tau}_1}$	$M_{\tilde{\tau}_2}$	$M_{\tilde{\chi}_1^\pm}$	$M_{\tilde{\chi}_2^\pm}$	$M_{\tilde{\chi}_1^0}$	$M_{\tilde{\chi}_2^0}$	$M_{\tilde{\chi}_3^0}$	$M_{\tilde{\chi}_4^0}$	$M_{\tilde{t}_1^0}$	$M_{\tilde{t}_2^0}$	$M_{\tilde{b}_1^0}$	$M_{\tilde{b}_2^0}$
5	300	114.7	190	155	206	138	272	88	142	208	272	373	645	406	508
15	300	120	189	151	209	146	267	89	148	212	226	373	645	448	515

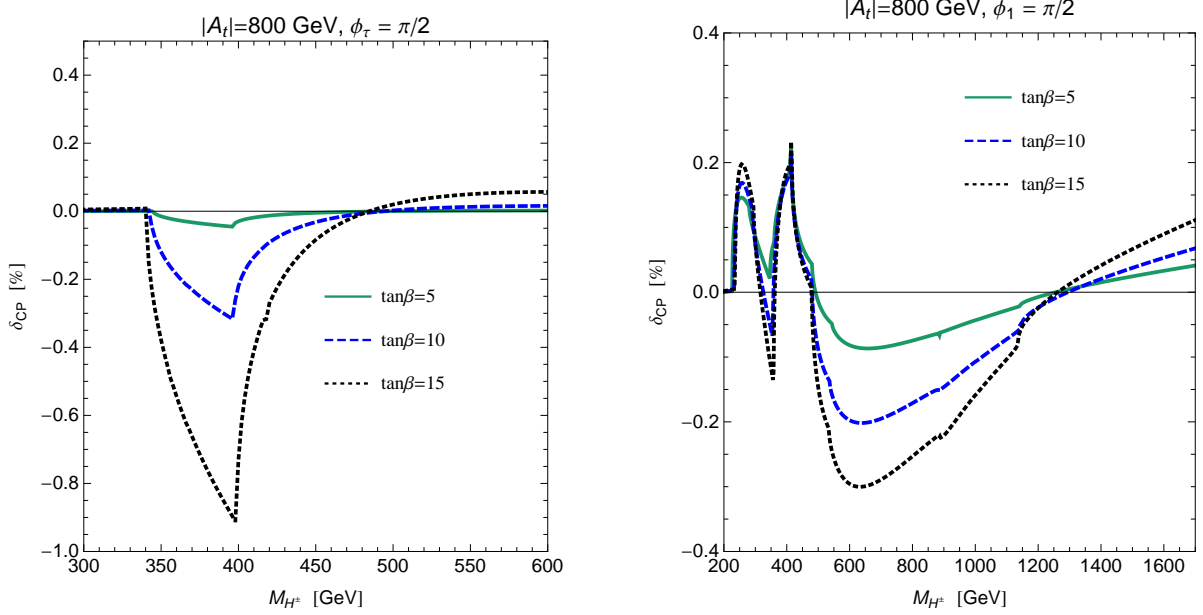


Figure 3:  $\delta_{\text{CP}}$  as function of the charged Higgs mass. The left panel is for  $\phi_\tau = \pi/2$  while the right panel is for  $\phi_1 = \pi/2$ . The solid, dashed and dotted lines are for  $\tan \beta = 5, 10$  and  $15$ , respectively.

mass constraint  $M_{h_1} > 114.5$  GeV for the lightest neutral Higgs particle (although for the complex MSSM the limits for the neutral Higgs bosons are less severe than in the real MSSM) and the experimental limits on the SUSY particles. In the following analysis, we will vary the trilinear couplings  $|A_{\tau/t/b}|$  to show their impact on the asymmetry. Since we use the  $\overline{\text{DR}}$  scheme for  $\tan \beta$  and the Higgs fields, our results depend on the renormalization scale  $\mu_R$ ; more details will be given in section 4.6. We chose  $\mu_R = m_t$ , which is the default value in FeynHiggs.

### 4.3 Dependence on $\phi_\tau$ and $\phi_1$

We want to display the impact of individual phases on the CP asymmetry. We therefore keep the phase considered non-zero while all the others are put to zero. The dependence on the phases  $\phi_\tau$  and  $\phi_1$  was studied already in [2]<sup>1</sup>. As mentioned before, we improved

<sup>1</sup> For a comparison, we have used the same approximation and the same set of input parameters as in Ref [2]. Our results are in agreement with theirs for the case of  $\phi_\tau = -\pi/2$ ,  $\phi_1 = 0$ . For the case

the calculation by taking important loop contributions into the denominator, hence our numerical results are of two to three times smaller.

For  $\phi_\tau = \pi/2$ ,  $\delta_{\text{CP}}$  as functions of  $M_{H^\pm}$  with different values of  $\tan\beta$  are shown in the left panel of figure 3. The diagrams (b, c, f, g) in figure 2 with  $\tilde{\tau}$  and  $\tilde{\nu}_\tau$  loops yield a contribution to the CP violating term. Below the  $\tilde{\nu}_\tau\tilde{\tau}_1$  threshold at  $M_{H^\pm} \simeq 345$  GeV,  $\delta_{\text{CP}}$  is negligible, in spite of contributions from beyond-one-loop terms with the  $\mathbf{Z}$  factors. The high peaks correspond to the  $\tilde{\nu}_\tau\tilde{\tau}_2$  threshold at  $M_{H^\pm} \simeq 396$  GeV. Increasing  $\tan\beta$  leads to a rapid decrease of the denominator, owing to the decreasing tree-level coupling, which is the main reason for the strongly rising  $\delta_{\text{CP}}$ . With  $\tan\beta = 5$ , the largest value of  $\delta_{\text{CP}}$  is about 0.05%, however with  $\tan\beta = 15$ ,  $\delta_{\text{CP}}$  can go up to 0.91%.

For  $\phi_1 = \pi/2$ ,  $\delta_{\text{CP}}$  is shown in the right panel of figure 3. The diagrams (a, c, d, e) in figure 2, with neutralino and chargino loops, contribute to the CP violating term. There are five visible thresholds,  $\tilde{\chi}_1^\pm\tilde{\chi}_1^0$  at  $M_{H^\pm} \simeq 226$  GeV,  $\tilde{\chi}_1^\pm\tilde{\chi}_2^0$  at  $M_{H^\pm} \simeq 280$  GeV,  $\tilde{\chi}_1^\pm\tilde{\chi}_3^0$  at  $M_{H^\pm} \simeq 346$  GeV,  $\tilde{\chi}_1^\pm\tilde{\chi}_4^0$  at  $M_{H^\pm} \simeq 400$  GeV and  $\tilde{\chi}_2^\pm\tilde{\chi}_3^0$  at  $M_{H^\pm} \simeq 480$  GeV.  $\delta_{\text{CP}}$  can reach 0.3% above the  $\tilde{\chi}_1^\pm\tilde{\chi}_1^0$  threshold, in general, however, it is rather small.

#### 4.4 Dependence on $\phi_t$ and $\phi_b$

Significantly larger values of  $\delta_{\text{CP}}$  can occur when  $\phi_t$  and  $\phi_b$  are non-zero and the CP violating terms get contributions from diagrams with top and bottom squarks loops (figure 2). The left panel of figure 4 shows the CP asymmetry as a function of the charged Higgs mass for  $\phi_t = \pi/2$ . There are two visible thresholds,  $\tilde{t}_1\tilde{b}_1$  at  $M_{H^-} \simeq 873$  GeV and  $\tilde{t}_2\tilde{b}_2$  at  $M_{H^-} \simeq 1149$  GeV for  $\tan\beta = 5$ .

The CP asymmetry is sizeable both for  $M_{H^\pm}$  below and above the  $\tilde{t}_1\tilde{b}_1$  threshold, especially for larger values of  $\tan\beta$ . Below the  $\tilde{t}_1\tilde{b}_1$  threshold, the most important term contributing to the CP asymmetry is the interference between diagram (c) in figure 2 and the triangles with top and bottom quarks. Close to the threshold, the interference of the diagrams (b, f, g) in figure 2 and the tree diagram are dominant. We observe that the individual contribution from the H-W mixing diagrams and the triangles with same particles inside loops can be much larger than the Born-term at the  $\tilde{t}_i\tilde{b}_j$  thresholds. However, they carry opposite signs and are almost of the same order of magnitude. The sum of both can be comparable with the Born term and is very sensitive with respect to  $\phi_t$ ,  $|A_t|$  and  $\tan\beta$ .

Above the  $\tilde{t}_1\tilde{b}_1$  threshold,  $\delta_{\text{CP}}$  can become very large. It can rise up to -51.6% at  $M_{H^-}=1600$  GeV,  $\tan\beta=15$ . This is a common feature of charged Higgs decays, as mentioned in Ref [12]. Moreover,  $\delta_{\text{CP}}$  has a strong dependence on  $|A_t|$ , as one can see in the right panel of figure 4. The  $|A_t|$  range is compatible with  $M_{h_1} > 114.5$  GeV.

The impact of the phase  $\phi_b$  on  $\delta_{\text{CP}}$  is shown in figure 5. It can be sizeable above  $M_{H^-}$  around the  $\tilde{t}_1\tilde{b}_1$  threshold, however it is still small compared to the effect of the phase  $\phi_t$ . For  $|A_t| = 800$  GeV, the largest value of  $\delta_{\text{CP}}$  obtained for  $\tan\beta = 15$  is about 8% close to the  $\tilde{t}_2\tilde{b}_2$  threshold.

The dependence of the CP asymmetry on the phase of  $A_t$  is illustrated in figure 6a, where we present  $\delta_{\text{CP}}$  as a function of the charged Higgs mass with different values of

---

$\phi_\tau = 0$ ,  $\phi_1 = -\pi/2$ , we found a difference resulting from the coupling between neutral Higgs bosons and neutralinos,  $A_{lk}$  in eq. (A.3) of Ref. [2] where an extra factor 1/2 is present. Adapting this factor, we get agreement

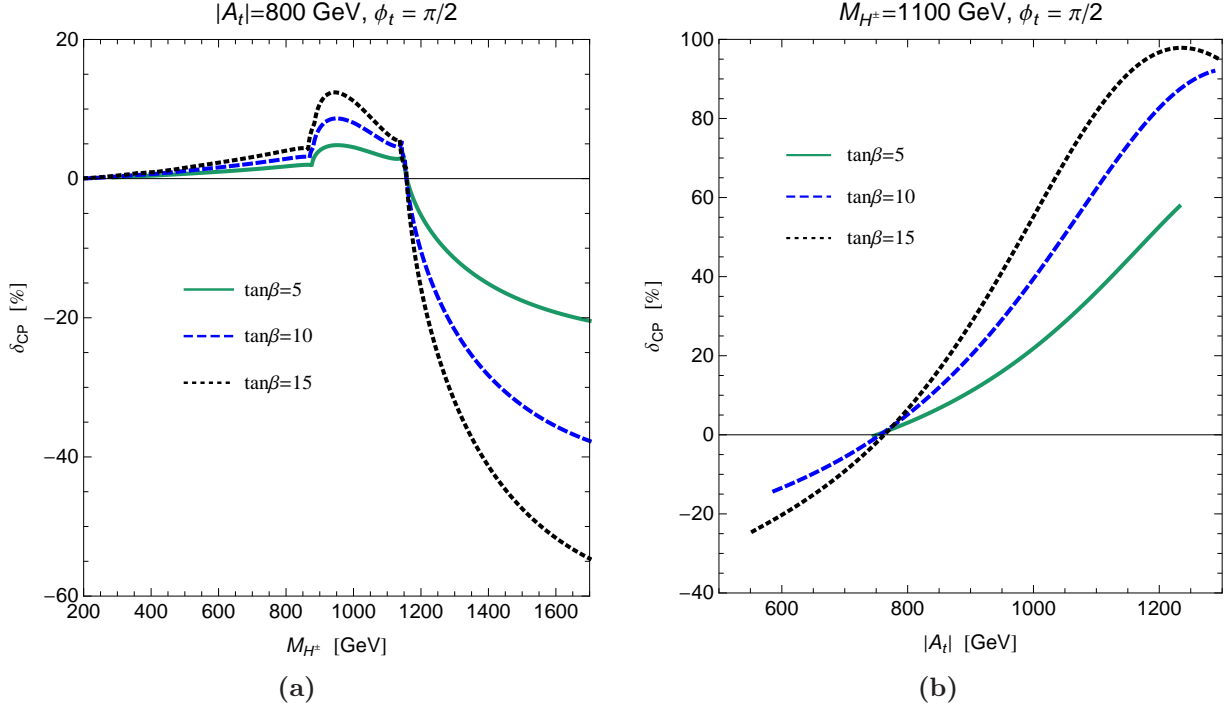


Figure 4: The CP asymmetry as functions (a) of the charged Higgs mass, (b) of  $|A_t|$ . The solid, dashed and dotted lines are for  $\tan\beta = 5, 10$  and  $15$ , respectively.

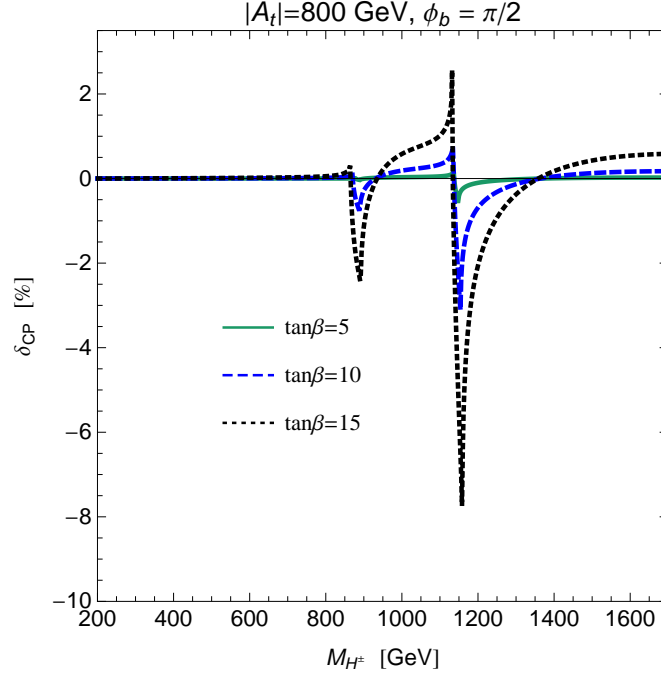


Figure 5: The CP asymmetry as function of charged Higgs mass, for  $\phi_b = \pi/2$ . The solid, dashed and dotted lines are for  $\tan\beta = 5, 10$  and  $15$ , respectively.

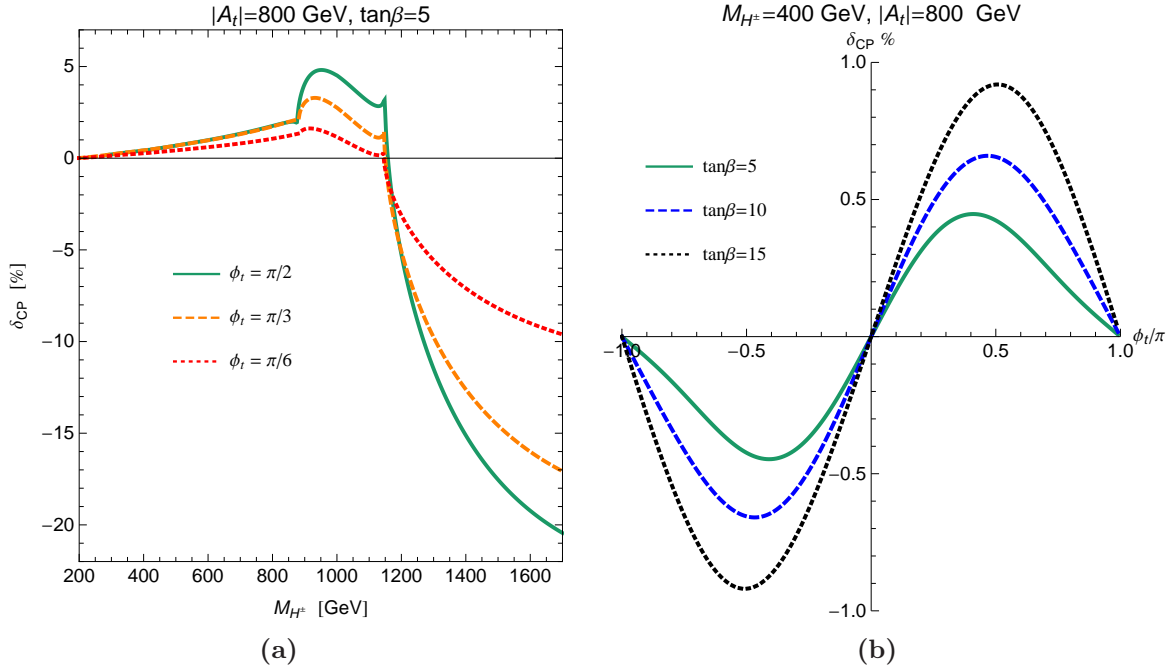


Figure 6: The CP asymmetry as function (a) of the charged Higgs mass for different values of  $\phi_t = \{\frac{\pi}{2}, \frac{\pi}{3}, \frac{\pi}{6}\}$  (b) of the CP asymmetry as functions the phase  $\phi_t$  for  $\tan\beta = 5, 10, 15$ .

$\phi_t = \frac{\pi}{2}, \frac{\pi}{3}, \frac{\pi}{6}$ . Figure 6b shows the CP asymmetry at  $M_{H^\pm} = 400$  GeV as a function of phase  $\phi_t$  with  $\tan\beta = 5, 10, 15$ . For  $\tan\beta = 15$  the maximum is at 0.92% for  $\phi_t = 0.51\pi$ . Compared to the contributions from  $\phi_1$  and  $\phi_\tau$  at low values of  $M_{H^\pm}$ , the impact of  $\phi_t$  on  $\delta_{CP}$  is considerably bigger, although not very strong from the absolute numbers.

As already mentioned, the sum of the decay widths for  $H^\pm \rightarrow W^\pm h_1$  is an important ingredient for  $\delta_{CP}$  and the Born approximation is in general insufficient. Therefore we address here the decay widths and branching ratios and the higher-order effects. For illustration we choose the decay  $H^- \rightarrow W^- h_1$ . In figure 7a, we show the Born, improved Born, improved one-loop and full decay widths, as described in section 3. The improved Born and improved one-loop decay widths are defined in (20) and (21). We choose  $\phi_1 = \phi_\tau = \phi_t = \phi_b = \pi/2$  for this analysis. For  $M_{H^\pm} = 300$  GeV, the one-loop vertex corrections can go up to 12.4% while at  $M_{H^\pm} = 1.6$  TeV corrections reduce to -35.4% compared to improved Born result. For low  $M_{H^\pm}$ , the improved one-loop and the full result are quite close to each other, but around and above the  $\tilde{t}_1 \tilde{b}_1$  threshold, the full result is clearly larger.

In figure 7b, we show the branching ratio of the decay  $H^- \rightarrow h_1 W^-$  for different values of  $\tan\beta$ , using the full decay width. The other relevant decays of the charged Higgs boson are computed in lowest order. For  $\tan\beta = 5$ , the branching ratio can reach 6.4% at  $M_{H^\pm} \simeq 219$  GeV. Around this point, the charged Higgs can decay mainly to  $tb$  and  $\tau\nu_\tau$ . When the mass of charged Higgs mass increases, the channels to charginos and neutralinos, stop and sbottom open. Thus, the branching ratio of  $H^- \rightarrow h_1 W^-$  drops rapidly, which makes it difficult to access  $\delta_{CP}$  experimentally. The branching ratio also depends strongly on the value of  $\tan\beta$ , especially for low values of  $\tan\beta$ , where the channels  $H^\pm \rightarrow h_1 W^\pm$  are

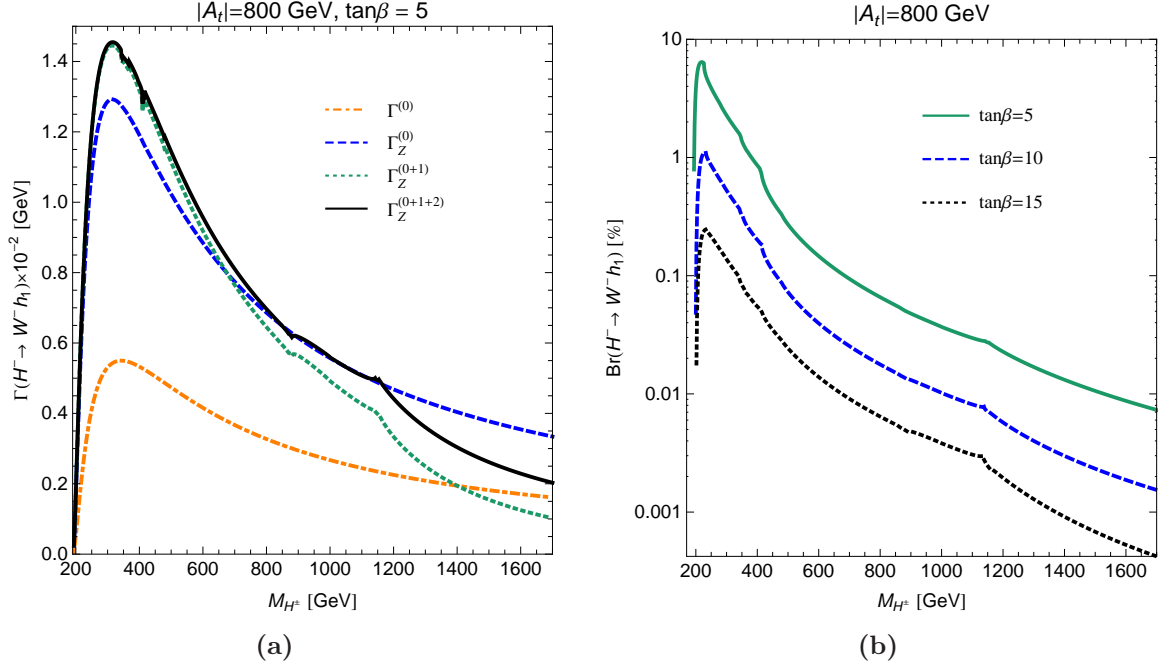


Figure 7: (a) The Born, improved Born, improved one-loop and full decay widths corresponding to dot-dashed, dashed, dotted and solid lines as functions of the charged Higgs boson mass. (b) The branching ratios of the decay  $H^- \rightarrow W^- h_1$  as functions of  $M_{H^-}$ , for  $\phi_1 = \phi_\tau = \phi_t = \phi_b = \pi/2$ .

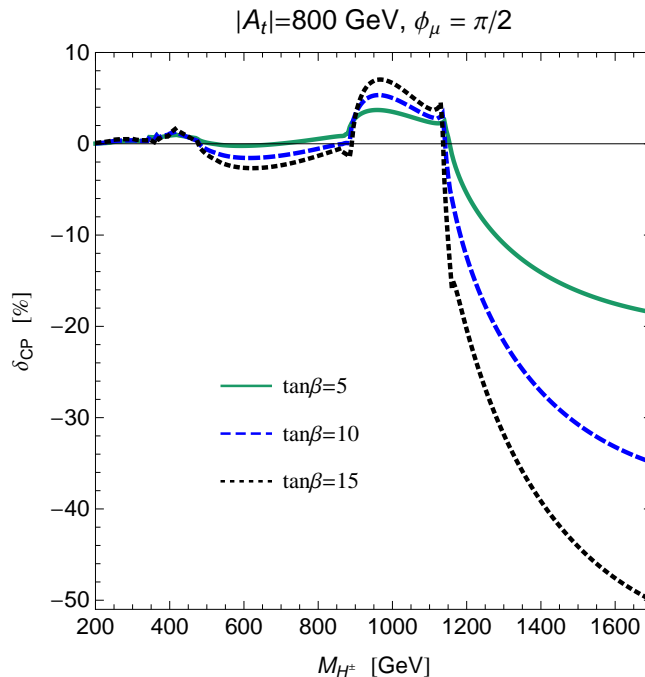


Figure 8: The CP asymmetry as functions of charged Higgs mass, for  $\phi_\mu = \pi/2$ . The solid, dashed and dotted lines are for  $\tan\beta = 5, 10$  and  $15$ , respectively.

interesting.

#### 4.5 Dependence on $\phi_\mu$

The phase of  $\mu$  is severely constrained by the experimental limits on the electric dipole moments of electron and neutron. This bounds can, however, be circumvented by a specific fine-tuning of the phases of  $\mu$  and of the non-universal SUSY parameters [13], leaving room also for a large phase  $\phi_\mu$ . We thus illustrate the effect of a large  $\phi_\mu$  on  $\delta_{\text{CP}}$  in Figure 8, which displays  $\delta_{\text{CP}}$  as a function of  $M_{H^\pm}$  for  $\phi_\mu = \pi/2$ . The CP violating part receives contributions from all diagrams in figure 2. For charged Higgs boson masses below the  $\tilde{t}_1\tilde{b}_1$  threshold, the main contribution to  $\delta_{\text{CP}}$  comes from the neutralino-chargino loops; above the threshold it is again dominated by the  $\tilde{t}_1\tilde{b}_1$  loops.

#### 4.6 Scale dependence

Here we comment on the dependence of the CP asymmetries on the renormalization scale  $\mu_R$ . Choosing a concrete example, Figure 9 shows  $\delta_{\text{CP}}$  versus of  $\mu_R$  at  $M_{H^\pm} = 400$  GeV and  $\tan\beta = 10$ . The dependence of  $\delta_{\text{CP}}$  on  $\mu_R$  comes mainly from the CP violating contribution in the numerator of (9). The strict one-loop contribution to the CP violating part of the decay width does not depend on  $\mu_R$  since it arises from the imaginary part of one-loop integrals. We however consider also higher-order terms, like the Higgs-mixing term  $\mathbf{Z}_{hA}M_A^{\text{tree}}\delta M_h$ , which depends on  $\mu_R$  through the  $\mathbf{Z}$  factors from the Higgs renormalization. For  $\phi_\tau$  and  $\phi_1$ ,

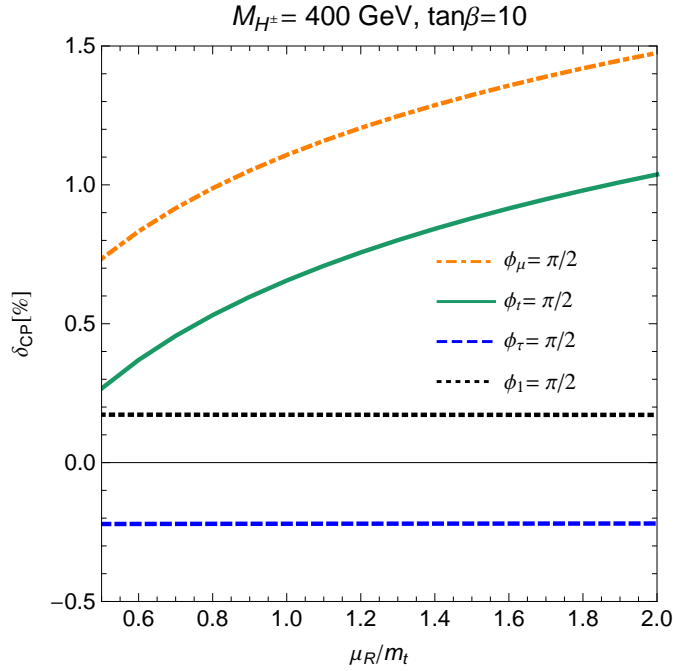


Figure 9: The CP asymmetry as functions of the renormalization scale for different phases.  $\mu_R$  is varied in the range  $[m_t/2, 2m_t]$ .

such terms are negligible and the dependence on  $\mu_R$  is irrelevant. For  $\phi_\mu$  and  $\phi_t$  they are more important, as one can see in the figure. For  $M_{H^\pm}$  values above the  $\tilde{t}_1\tilde{b}_1$  threshold, the one-loop contribution is the most important, and then the  $\mu_R$  dependence is much weaker.

#### 4.7 The CPX scenario

A case of particular interest is the CPX scenario where the SUSY parameters maximize the CP-violating effects due to the large value of the product  $\text{Im}(\mu A_t)/M_{\text{SUSY}}^2$  [14]. According to Ref. [15], we use the following set of on-shell parameters

$$\begin{aligned} \mu &= 2000 \text{ GeV}, M_{\text{SUSY}} = 500 \text{ GeV}, |A_f| = 900 \text{ GeV}, \\ M_3 &= 1000 \text{ GeV}, M_2 = 200 \text{ GeV}, M_1 = 5/3 \tan^2 \theta_W M_2. \end{aligned} \quad (24)$$

In figure 10a, we display the CP asymmetry caused by the complex phase of  $A_t$  for  $\tan \beta = 5, 10, 15$ . As one can see,  $\delta_{\text{CP}}$  is quite large both below and above  $\tilde{t}_1\tilde{b}_1$  threshold. For  $\tan \beta = 5$ ,  $\delta_{\text{CP}}$  is about -6% at  $M_{H^\pm} \simeq 400 \text{ GeV}$  and can reach 100% at  $M_{H^\pm} \simeq 1116 \text{ GeV}$ . In figure 10b, the decay width is shown as function of  $M_{H^\pm}^\pm$ . Note that above the  $\tilde{t}_1\tilde{b}_1$  threshold, the one-loop correction becomes very large, making the improved one-loop width negative, which demonstrates that this kind of approximation is unphysical and shows the importance of not truncating the squared amplitude.

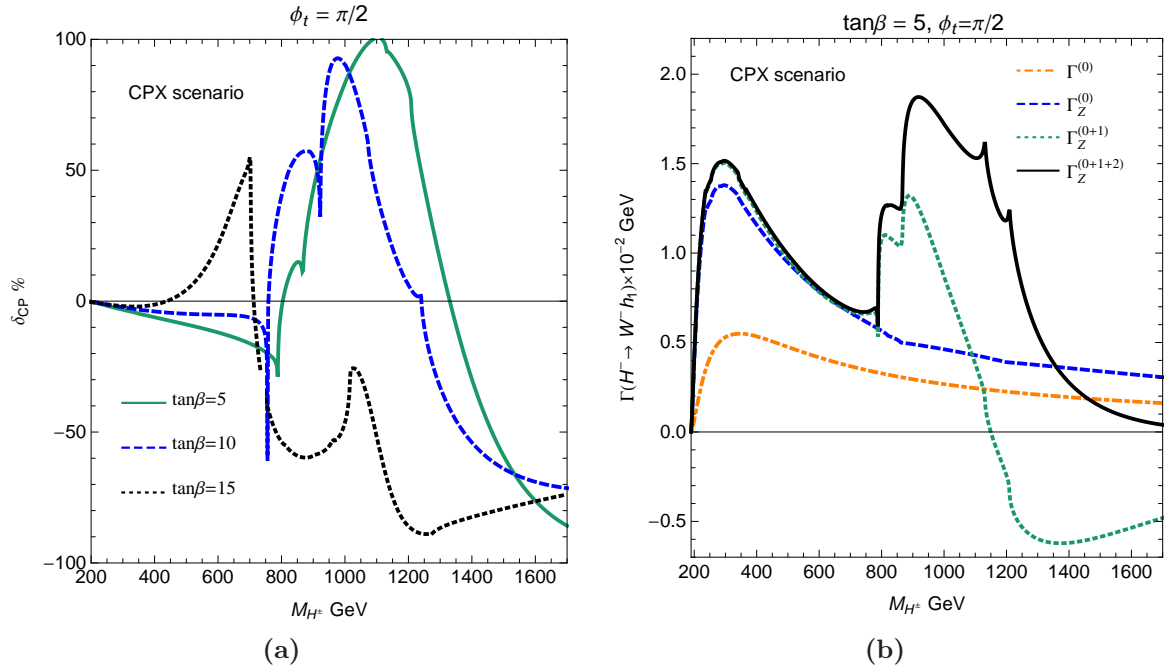


Figure 10: (a)  $\delta_{\text{CP}}$  as function of the charged Higgs mass in the CPX scenario. (b) The Born, improved Born, improved one-loop and full decay widths, corresponding to dot-dashed, dashed, dotted and solid lines, as functions of the charged Higgs mass in the CPX scenario.

## 5 Conclusions

We have calculated the CP violating asymmetry from the decays  $H^\pm \rightarrow h_1 W^\pm$  originating from non-vanishing complex phases in the complex MSSM. All the phases that can give sizable contributions to  $\delta_{\text{CP}}$  are taken into account and discussed. The impact of the phases  $\phi_\tau$ ,  $\phi_1$  and  $\phi_b$  on CP rate asymmetry is of some significance only above the threshold. The phase  $\phi_t$  can yield large contributions to the CP asymmetry both below and above the thresholds.  $\phi_t$  and  $\phi_\mu$  can induce large  $\delta_{\text{CP}}$  at large  $M_{H^\pm}$ .  $\delta_{\text{CP}}$  depends strongly on  $M_{H^\pm}$ ,  $|A_t|$  and  $\tan\beta$ .

We have also presented the decay width and the branching ratio of the decay  $H^- \rightarrow h_1 W^-$ . They turn out to be significant in particular for small values of  $\tan\beta$  and low masses of the charged Higgs boson. With increasing mass they become rather small.

Although the CP asymmetry can be large, the small branching ratios make the experimental observability quite difficult. A characteristic number for a feasibility estimate is the quantity  $N = (\delta_{\text{CP}}^2 \times \text{Br})^{-1}$  [16], the number of the (at least) required charged Higgs bosons to be produced for observing the CP asymmetry. For  $M_{H^\pm} = 500$  GeV and an asymmetry of  $-9\%$ , as in the CPX scenario for  $\tan\beta = 5$  with a branching ratio of  $4.2\%$ , one would need about  $N = 3 \cdot 10^3$ . At the Large Hadron Collider (LHC) the dominant production occurs through the partonic process  $g b \rightarrow t H^-$  (see e.g. [17] for a review), which with a cross section of  $19$  fb could provide such a number of charged Higgs bosons for an integrated luminosity of  $160 \text{ fb}^{-1}$ . Considering a very large asymmetry of  $0.9$  as for  $M_{H^\pm} = 1000$  GeV, one has to cope with a very small branching ratio of  $6.7 \cdot 10^{-4}$ , requiring  $N = 1.9 \cdot 10^3$ ; for a



production cross section of 1.2 fb a luminosity of more than  $1.6 \cdot 10^3 \text{ fb}^{-1}$  would be needed, which is outside the scope of the LHC with the envisaged design luminosity (but might be of interest for an upgraded SLHC).

For a more realistic study, moreover, one has to take into account that CP violating effects are also part of the main production processes  $g b(\bar{b}) \rightarrow t H^- (\bar{t} H^+)$  [18], which makes a complete calculation for  $H^\pm$  production and decay at NLO necessary.

At a Linear Collider, the basic production process  $e^+ e^- \rightarrow H^+ H^-$  has the advantage of providing a symmetric state, from which the observation of CP violation in the charged Higgs decays might look more promising, but is also depleted by low production rates and branching ratios. The cross section for pair production with  $M_{H^\pm} = 500 \text{ GeV}$  at a center-of-mass energy of 3 TeV (CLIC) is 2.6 fb, which would require an integrated luminosity of  $1.2 \cdot 10^3 \text{ fb}^{-1}$ . For lower Higgs masses (up to 400 GeV), one can expect higher production rates at a 1 TeV collider, but the predicted CP asymmetries are rather small in that range.

## Acknowledgements

We would like to thank Santiago Bejar Latonda and David Lopez Val for cross-checking some parts of our calculations and Le Duc Ninh and K.E. Williams for fruitful discussions.

## References

- [1] E. Accomando *et al.*, *Workshop on CP Studies and Non-Standard Higgs Physics*, eds. S. Kraml et al., CERN 2006-009, arXiv:hep-ph/0608079.
- [2] E. Christova, E. Ginina and M. Stoilov, JHEP **0311** (2003) 027 [arXiv:hep-ph/0307319].
- [3] M. Frank, T. Hahn, S. Heinemeyer, W. Hollik, H. Rzehak and G. Weiglein, JHEP **0702** (2007) 047 [arXiv:hep-ph/0611326].
- [4] S. Bejar, W. Hollik, D. Lopez-Val, *The  $Wh_1$  decay mode of the charged Higgs boson: a complete 1-loop analysis*, to appear
- [5] J. Kublbeck, M. Bohm and A. Denner, Comput. Phys. Commun. **60** (1990) 165.  
T. Hahn, Comput. Phys. Commun. **140** (2001) 418 [arXiv:hep-ph/0012260].  
T. Hahn and C. Schappacher, Comput. Phys. Commun. **143** (2002) 54 [arXiv:hep-ph/0105349].
- [6] T. Hahn and M. Perez-Victoria, Comput. Phys. Commun. **118** (1999) 153 [arXiv:hep-ph/9807565].  
G. J. van Oldenborgh and J. A. M. Vermaseren, Z. Phys. C **46** (1990) 425.
- [7] T. Hahn, S. Heinemeyer, W. Hollik, H. Rzehak and G. Weiglein, Comput. Phys. Commun. **180** (2009) 1426.  
S. Heinemeyer, W. Hollik and G. Weiglein, Comput. Phys. Commun. **124** (2000) 76 [arXiv:hep-ph/9812320].  
S. Heinemeyer, W. Hollik and G. Weiglein, Eur. Phys. J. C **9** (1999) 343 [arXiv:hep-ph/9812472].  
G. Degrandi, S. Heinemeyer, W. Hollik, P. Slavich and G. Weiglein, Eur. Phys. J. C **28** (2003) 133 [arXiv:hep-ph/0212020].
- [8] B. A. Kniehl, C. P. Palisoc and A. Sirlin, Nucl. Phys. B **591** (2000) 296 [arXiv:hep-ph/0007002].
- [9] C. Amsler *et al.* [Particle Data Group], Phys. Lett. B **667** (2008) 1.
- [10] [Tevatron Electroweak Working Group and CDF Collaboration and D0 Collab], “Combination of CDF and D0 Results on the Mass of the Top Quark,” arXiv:0903.2503 [hep-ex].
- [11] M. S. Carena, S. Heinemeyer, C. E. M. Wagner and G. Weiglein, “Suggestions for improved benchmark scenarios for Higgs-boson searches at LEP2,” arXiv:hep-ph/9912223.
- [12] E. Christova, H. Eberl, W. Majerotto and S. Kraml, Nucl. Phys. B **639** (2002) 263 [Erratum-ibid. B **647** (2002) 359] [arXiv:hep-ph/0205227].  
A. Arhrib, R. Benbrik and M. Chabab, Acta Phys. Polon. Supp. **1** (2008) 417 [arXiv:0710.3555 [hep-ph]]

- [13] T. Ibrahim and P. Nath, Phys. Rev. D **57**, 478 (1998) [arXiv:hep-ph/9708456].  
M. Brhlik, G. J. Good and G. L. Kane, Phys. Rev. D **59**, 115004 (1999) [arXiv:hep-ph/9810457].  
A. Bartl, T. Gajdosik, W. Porod, P. Stockinger and H. Stremnitzer, Phys. Rev. D **60**, 073003 (1999) [arXiv:hep-ph/9903402].
- [14] M. S. Carena, J. R. Ellis, A. Pilaftsis and C. E. M. Wagner, Phys. Lett. B **495** (2000) 155 [arXiv:hep-ph/0009212].
- [15] K. E. Williams and G. Weiglein, Phys. Lett. B **660** (2008) 217 [arXiv:0710.5320 [hep-ph]].
- [16] G. Eilam, J. L. Hewett and A. Soni, Phys. Rev. Lett. **67** (1991) 1979.
- [17] A. Djouadi, Phys. Rept. **459** (2008) 1 [arXiv:hep-ph/0503173].
- [18] E. Christova, H. Eberl, E. Ginina and W. Majerotto, Phys. Rev. D **79**, 096005 (2009) [arXiv:0812.4392 [hep-ph]].